Beyond winglets: evolution of flight-related morphology in stick insects (Phasmatodea)

Yu Zeng[1,2†], Sehoon Park[1], Camille Gonzales[1], Faszly Rahim[3,4], and Robert Dudley[1,5]

[1]Department of Integrative Biology, University of California, Berkeley, CA 94720, USA
[2]Schmid College of Science and Technology, Chapman University, Orange, CA 92866, USA
[3]Centre for Insect Systematics (CIS), Universiti Kebangsaan Malaysia, 43600 Bangi, Selangor, Malaysia
[4]Islamic Science Institute (ISI), Universiti Sains Islam Malaysia, 71800 Bandar Baru Nilai, Negeri Sembilan, Malaysia
[5]Smithsonian Tropical Research Institute, Balboa, Republic of Panama
†Corresponding author: dreavoniz@berkeley.edu

Acknowledgments: We thank Francis Seow-Choen for helping with field work and commenting on stick insect natural history. We also thank David Wake, Paul Brock, Kipling Will, Rosie Gillespie and George Roderick for comments, and thank Faye Pon, Joan Chen, Stephanie Yom, Xiaolin Chen, Ho-Yeon Han, Ian Abercrombie, Yamai Shi-Fu Huang, Lin Cao, Azuan Aziz, and Juhaida Harun for help with data collection. We further thank the Forestry Department of Pahang, Malaysia, for permission to collect insects. This research was supported by National Science Foundation (DDIG-1110855), the Museum of Vertebrate Zoology and the Department of Integrative Biology at UC-Berkeley, the Undergraduate Research Apprentice Program (URAP) of UC-Berkeley, the Society for Integrative and Comparative Biology (SICB), and the Ministry of Higher Education Malaysia [FRGS/1/2012/SG03/UKM/03/1(STWN)].

Author contributions: Y.Z. devised experiments and performed the majority of data collection and analyses. S.P. and C.G. contributed to data collection and morphological analyses, and F.H. contributed to field data collection. Y.Z. and R.D. contributed to writing of the manuscript.

Conflicts of Interests: The authors declare no conflicts of interests.

Beyond winglets: evolution of flight-related morphology in stick insects (Phasmatodea)

Abstract

The first winged insects evolved from a wingless ancestor, but details of the transition from wingless to winged morphology remains unclear. Studying extant pterygotes undergoing secondary flight loss may help to understand such a transition in reverse temporal sequence. Stick insects (Order Phasmatodea) exhibit differently sized partial wings and frequent transitions between fully-winged and wingless forms, along with robust near-isometric scaling of wing area and body mass, with a correspondingly wide range of wing loading variation. To address how other flight-related morphological traits (including the flight apparatus and body-leg system) might correlate with wing size evolution, we studied wing and body shape in fifty different phasmid taxa over a wing loading range from 1.4 – 2300 Nm^{-2}. Wing shape evolution showed sex-specific trends, with a linear reduction of aspect ratio over the wing loading range of 2.2 – 23 Nm^{-2} in female insects, but a positive correlation with wing size in the males. Also, with reduced wing size and increased wing loading, wing venation exhibited structural reconfiguration across the wing loading range 6 – 25 Nm^{-2}, and the wingbase shifted from the anterior half of the body to nearer the center of body mass. Nonetheless, masses of the wings and flight muscle, and the shape of the body-leg system, were predominately predicted by specific allometric scaling relationships and not by wing loading. Such morphological reorganization relative to wing size evolution likely reflects interplay between selection on flight performance and on wing and body size within different ecological contexts. These results reveal complex reconfiguration of flight-related traits on the wing loading landscape during wing and body size evolution in phasmids.

Keywords

allometry, flightlessness, legs, sexual dimorphism, venation, wings

1. Introduction

Deriving from a single phylogenetic origin, pterygotes and their wings continue to exhibit rich dynamics on evolutionary timescales. The ancestors of winged insects were small terrestrial hexapods possessing only protowings (see Kukalová-Peck, 1983; Ellington, 1991; Dudley, 2000). And although the initial process of flight gain remains unclear, the earliest winged insects must have undergone substantial increase in wing size under selection. Once equipped with substantial wings, numerous pterygote lineages have then secondarily undergone partial or complete wing loss; ~5% of the extant pterygote fauna is flightless (Roff, 1994). The main reason underlying secondary flight reduction is likely the energetic cost for developing and maintaining the flight apparatus (e.g., wings and associated musculature), along with high energy expenditure during flight. Partial reduction or complete loss of wings has been associated with various ecological conditions, including developmental tradeoffs, enhanced female fecundity, and reduced demand for aerial mobility in montane habitats (Roff, 1994; Mani, 2013).

Partial wings presumably possess reduced aerodynamic capabilities (e.g., force generation) but may still serve locomotor functions within specific behavioral contexts, which has only been reported in derived taxa (e.g., water surface skimming in stoneflies; Marden, 2003). More often, size-reduced wings serve secondarily derived non-aerodynamic functions, such as use in protection, stridulation, and startle displays (see Dudley, 2000). Notably, one understudied behavioral context is controlled aerial descent (including parachuting and gliding). Empirical analyses suggest that flapping flight by pterygotes may have evolved from gliding in apterygotes via a series of intermediate morphologies with partial wings (Dudley et al., 2007; Dudley and Yanoviak, 2011). Within such a context, partial wings on a stably falling insect will interact with an upward flow field, and thus would be subject to high aerodynamic loading (Zeng et al., 2017).

A systematic examination of the transition in flight-related morphology between winged and wingless forms may help to understand the biomechanical origins of insect flight. Such an investigation may be approached at two levels. First, it is important to address features of the flight apparatus, including the wings and flight muscle, with respect to variation in relative wing size. For example, the shape and flexibility of wings are biomechanically coupled with the aerodynamics of flapping wings and body movements during flight. For fully winged insects, wing shape is often sexually dimorphic and may vary with species-specific ecology (e.g., Le Roy et al., 2019; Perrard et al., 2014); greater variation may be expected if the insects undergo drastic loss of flight capability. Also, because partial wings may interact with air flow differently than do full-sized flapping wings, the pterothoracic morphology and flight musculature may be reconfigured to power specific wing motions. Second, it is important to address the morphology of the body-leg system. The body-leg system is conventionally treated as the ‘airframe’ with legs omitted, but the legs are fully extended in many flying insects and thus should be incorporated aerodynamically. The body-leg system influences flight via both aerodynamic and inertial forces, which are determined by the size, shape, and mass of individual segments and their joint configurations (see Dudley, 2000). For species with partial wings, the body-leg system may serve as the dominant aerodynamic surface, assisting force production or stability via postural control and movements (Thomas and Taylor, 2001).

The stick insects (Order Phasmatodea) represent one of the few pterygote clades that have been analyzed for wing size variation within a context relevant to flight biomechanics. These insects are herbivorous and generally inhabit terrestrial vegetation, including tall tree canopies. Extant phasmids exhibit vestigial forewings and variably-sized hindwings (denoted the ‘wings’ hereafter), ranging from fully-sized to almost absent or vestigial wings. The processes of wing reduction and flight transition in phasmids remain largely understudied, despite the hypothesis that relaxed selection for flight (i.e., aerodynamic utility) underpins short-winged or wingless species within an arboreal context (Zeng et al., 2020). A recent study showed ascending flight in leaf insects, a group of leaf-mimicking phasmids (Boisseau et al., 2022).

Previous work revealed robust near-isometric scaling laws of body mass and wing area in stick insects, which allows for a relatively confident prediction of wing loading (p_w; the average pressure exerted on air by the wings) using body length (L) and the relative wing size (Q; i.e., the ratio of absolute wing length L_w to L). The empirical prediction for wing loading is a surface defined by L and Q (the 'wing loading landscape'), which enables analysis of trait variation with respect to different stages of flight loss (**Fig. 1A**; Zeng et al., 2020). By analyzing species richness of different flight morphologies, this study revealed two 'adaptive peaks' among winged stick insects: one was associated with long-winged species with a relative wing size $Q \approx 0.7$, and the other with species with miniaturized wings of $Q < 0.3$ used for non-aerodynamic functions (e.g., visual display). These two peaks were separated by an 'adaptive valley' of short-winged species with $Q \approx 0.3$ and $p_w \approx 10$ Nm^{-2}. The morphological space characterized by $p_w <$ ~10 Nm^{-2} thus characterizes a continuous reduction of flight capability as wing loading increases. Furthermore, p_w, L, and Q are evolutionarily coupled but each may subject to different selective pressures. The most general pattern was an inverse correlation between Q and L (i.e., smaller body with larger wings, or the converse) in both female and male stick insects (**Fig. 1B,C**). Selection for dispersal efficiency has probably favored lower wing loading in males, whereas selection for fecundity has likely driven body size increase and wing reduction in females (see Zeng et al., 2020).

Here, we examine the evolution of flight-related morphology beyond these correlations between L and Q. Because there was no prior study on the flight of partial-winged insects, we derive our hypotheses based on predictions from controlled descent of wingless insects (Zeng et al., 2017). We hypothesize that: (i) with increasing wing loading, taxa would exhibit changes in wing morphology (i.e., both shape and venation) to offset increased aerodynamic loading; and (ii) the body-leg system may be reconfigured to benefit stability. We first examined the scaling of wing shape, venational pattern of wings, and masses of wings and flight musculature with respect to p_w, L, Q, and the absolute wing length L_w (= LQ). Specifically, we adopted simplified geometric models and performed sensitivity analyses to identify potential variation associated with the aforementioned 'adaptive valley' near p_w ~10 Nm^{-2}. We also examined mass distribution, projected planform area, and the longitudinal position of relevant joints for the body-leg system.

We assessed two phylogenetic levels within the Phasmatodea. The first analyzed interspecific variation with a pool of 50 taxa composed of both males and females from major clades, and covering a wing loading range of 1.4 – 2300 Nm^{-2} (**Fig. 1B,C**; **SI Fig. S1A**). At the sub-species level, we examined the tropical stick insect *Asceles tanarata* Brock, 1999. *A. tanarata* represents one of the few well-documented cases of discrete intraspecific variation in flight-related morphology across an environmental gradient. *A. tanarata* is native to the Malay Peninsula (Brock, 1999; Seow-Choen, 2000), and consists of three subspecies distributed along an altitudinal gradient from ~50 m to ~1600 m, with a wing reduction ranging from fully developed to miniaturized wings, along with substantial body size reduction (**Fig. 1D,E**). This species group exhibits a unique coupled reduction in wing and body size, which is an outlier for stick insects considering the more general inverse correlation between wing and body sizes (**Fig. 1B,C**). For simplicity, the six study morphs are coded numerically in order of increasing altitudinal occurrence (i.e., *A. tanarata singapura*, At1; *A. tanarata amplior*, At2; *A. tanarata tanarata*, At3), and with the suffixes 'f' and 'm' denoting 'female' and 'male', respectively.

2. Materials and methods

2.1 Insect collection and husbandry

We sampled 56 taxa (26 females and 30 males from 47 species; 0.2 < Q < 0.85) from field-captured or captive-reared insects (**SI Data S1**). Analysis of wing and body morphometrics followed Ellington (1984). For the *A. tanarata* group, insects were collected on host plants (*Macaranga* spp. and *Melastoma* spp.) at type localities (**Fig. 1E**) during night expeditions (August 2008, July 2010 and August 2011). Before experimental treatments, individual insects were maintained in large plastic containers with fresh leaves from host plants, and were held in an air-conditioned room at 22 – 26 °C.

2.2 Morphometrics

To analyze wing morphology, we took images of fully unfolded hind wings using a digital camera (Olympus E-3) (N = 34 female taxa; N = 36 male taxa). Insects were anesthetized either with a 5-min cold treatment (0–4 °C) or a 5-min CO_2 treatment. Two-dimensional images of wings were then extracted using Photoshop (Adobe Inc., USA), and were measured using ImageJ (Abràmoff et al., 2004) for lengths (L_w) and areas (A_w) (**SI Fig. S1D**). Wing shape descriptions followed previous methods (Ellington, 1984). Relative wing size was calculated as $Q = \frac{L_W}{L}$, where L_W is wing length and L is body length. Wing loading was calculated as $p_w = \frac{mg}{2A_w}$, where m is insect mass, g is gravitational acceleration and A_w is the wing area (see also Zeng et al., 2020).

Identification of primary radial veins followed Ragge (1955), where the anterior anal (AA) and posterior anal (PA) veins were identified using associations with axillary sclerites at wingbase (**SI Fig. S1B**). The variation of the number of AA veins (N_{AA}) with respect to p_w was fitted with inverse sigmoid curves using a Four Parameter Logistic Regression (R package 'dr4pl'; Ritz et al., 2015) as:

$$n_{AA} = \frac{a - d}{1 + \left(\frac{p_W}{c}\right)^b} + d \quad (1)$$

where a, b, c, and d are the four fitting coefficients.

Body sections and legs were treated as a system of cylinders, including the anterior body section (BS1) and posterior body section (BS2) as connected at the median joint (i.e., the 1st abdominal tergum; Bragg, 1997), and the six legs (see **SI Fig. S1D**). To obtain projected planforms of body and leg segments, anesthetized insects were laid dorsoventrally on a flat surface with their legs fully extended for digital imaging. Two-dimensional images of all body parts were then extracted using Photoshop (Adobe Inc., USA), and were measured using ImageJ (Abràmoff et al., 2004) for lengths and planform areas.

2.3 Mass of flight muscle

Flight muscle mass was measured in a total of 16 different flight morphs (6 females and 4 males from six species reared in the laboratory and 3 females and 3 males of the *Asceles tanarata* species group collected in the field), covering a relative wing size range from 0 – 0.78, with 2 – 6 individuals per flight morph (see **SI Data S1**). We first cut off the metathorax from euthanized insects and removed muscles associated with hindlegs and the median joint. We then indirectly measured the mass of flight muscles following NaOH digestion of soft tissue, with duration of chemical treatment adjusted according to the size of wings (Q > 0.5, 12 hr; 0.3 < Q < 0.5, 2 hr; Q <0.3, 30 min).

2.4 Mass distribution of body-leg system

The masses of two body sections and the legs were measured from deep-frozen specimens in **20** taxa (10 females and 10 males) from **12** species either reared in the laboratory or collected in the field (**SI Data S1**). Each body part was cut from frozen specimens and measured with a portable electronic balance (PP-2060D, Acculab; accuracy of 0.001 g and linearity of ±0.004 g) in the field or with an electronic balance (R200D, Sartorius AG, Germany) in the lab. The center of mass (COM) of the body (i.e., of the head, thorax, and abdomen) was estimated from images of frozen specimens (with legs removed) balanced on a vertically oriented razor blade (**SI Fig. S1E**). Wing mass was measured from freshly euthanized specimens. Forewings were highly reduced in size (i.e., < 5% A_w and < 0.1% mass in all sampled taxa) and were thus omitted.

The total leg mass ranged from 9% – 24% of body mass (see **SI Data S1**) and was included in corresponding body sections. Based on observations of leg posture in flight (**SI Fig. S1D**), the mass of fore- and mid-legs was included in the anterior section, and the mass of the hind-legs was included in the posterior section. The longitudinal position of the COM relative to the anterior end was calculated as:

$$P_{COM} = \frac{0.5L_1 + (L_1 + 0.5L_2)r_m}{1 + r_m} \quad (2)$$

where L is the length of a body section, subscripts 1 and 2 denote the anterior and posterior sections, respectively, and $r_m (= m_2/m_1)$ is the mass ratio of the posterior to the anterior section. The moment of inertia (MOI) of the abdomen about the insect's COM was calculated as $I = m_2 r^2$, where r is the distance from m_2 to the COM.

2.5 Statistical analyses

For phylogenetically justified correlations, we used a molecular phylogeny that includes all three subspecies of the *A. tanarata* from a previous study (**SI Fig. S1A**; Zeng et al., 2020). The phylogenetic signals for wing and body size were significant. For the species lacking molecular data, we added them as polytomous tips to the node representing the latest common ancestor on the tree. We then generated 100 random trees with randomly resolved polytomous tips. Each new node was added using the function 'multi2di' (package 'ape'; Paradis et al. 2004), and was given a branch length that was randomly drawn from a normal distribution of branch lengths with a mean of 0.1 × mean branch lengths of the original tree, and a standard deviation of 0.01 × the standard deviation of branch lengths from the original tree. We then conducted phylogenetic generalized least square (PGLS) analyses (package 'caper'; Orme et al., 2013) and ordinary generalized least square analyses (GLS). For each correlation, we ran PGLS on all random trees and summarized the results (MLλ and coefficients), which were then compared with those from GLS tests conducted without reference to the phylogeny (i.e., λ = 0).

For correlations of a given trait with respect to wing loading, we conducted sensitivity analyses using a series of generalized linear regressions to identify the potential p_w value corresponding to a critical transition in the trait. With custom-written scripts in R, we first generated a series of p_w ranges with different upper limits (denoted $p_{w(max)}$). We then examined the significance of correlations (i.e., standard errors and *P*-values of slope coefficients) with respect to p_w.

3. Results

3.1 Evolution of wing shape

Among all examined taxa, wing aspect ratio (AR) varied between 1.2 and 2.7 (male, 1.6 – 2.6; female, 1.2 – 2.7). Wings of high AR (> 2) were generally found in insects with wing loading < 10 Nm^{-2}, whereas low AR (< 1.5) was associated with female wings in the p_w range of 5 – 10 Nm^{-2} (**Fig. 2A**). The variational pattern of AR was specific to each sex. Wing AR was not correlated with body size in either sex (**SI Table S1**). On one hand, female wing AR exhibited a reduction with increasing p_w, as shown by a progressively rounder wing shape (**Fig. 2A**). Based on sensitivity analysis, this reduction corresponds to the lower limit of p_w ~2.2 Nm^{-2}, and to an upper limit of ~23 Nm^{-2} (**Fig. 2B**). On the other hand, male wing AR varied between 1.6 – 2.3 and was positively correlated with absolute wing length L_w (**Fig. 2C**). These evolutionary patterns in wing shape suggest significant selection for wing aerodynamic function, potentially coupled with a sex-specific body plan and flight biomechanics (see **Discussion**).

3.2 Evolution of wing venation

The first general pattern we noticed was that the number of primary radial veins was coupled with wing size, as demonstrated with exemplar wings (**Fig. 3A**). Note that female insects had more radial veins than the males with same wing loading, corresponding to a relatively greater mass allometry exponent (see Zeng et al., 2020). With PGLS analyses, we found the total number of radial veins (N_V) was more significantly correlated with wing loading and with relative wing size Q than with absolute wing size L_w (**Fig. 3B**; **SI Table S1**). With a structural design resembling a 'Chinese fan', wing length mainly equaled the length of elytrized costal veins and was also close to the length of the longest (and most costal) radial veins (AA1); it thus was not coupled with the number of radial veins, duplication of which mainly determine wing shape and chord size. As expected, the scaling exponent of N_V with L_w was only ~0.3.

The second general pattern was that the number of anterior anal (AA) veins was relatively conserved, whereas that of the posterior anal (PA) veins decreased more sharply with reduced wing size. Correspondingly, the AA veins supported the membrane region adjacent to the elytrized costal edge, whereas the PA veins supported the more posterior anal region. The number of PA veins (N_{PA}) varied between 2 – 14, exhibiting a linear correlation with p_w (**Fig. 3C**). The number of AA veins (N_{AA}) only varied between 5 – 7, which were well fitted with inverse sigmoid curves using Four Parameter Logistic Regression models and which showed sharp reductions at $p_w \approx 10$ Nm^{-2}. (**Fig. 3D**). Treating the midpoint $N_{AA} = 6$ as a critical transition, the regression models predicted the corresponding critical p_w values to be $10^{0.75}$ Nm^{-2} (i.e., 5.8 Nm^{-2}; confidence interval of 4.4 – 8.1 Nm^{-2}) for males and $10^{1.3}$ Nm^{-2} (i.e., 18.4 Nm^{-2}; confidence interval ~0 due to small sample size of $N_{AA} = 6$) in females (**SI Data S1**). With a prediction for the function of two vein groups, and especially for structural support in the downstroke by AA veins, this pattern of vein reorganization and reduction is likely coupled with changes in wing aerodynamics at low to medium-high values of wing loading (see **Discussion**).

Furthermore, as inter-vein angles are relatively conserved (e.g., 6.8˚ – 8.8˚ between radial veins in *A. tanarata*; see **SI Fig. S3D**), the gap size (or transverse distance) between adjacent veins should increase toward the wing margin, with greater distances in longer wings. Probably so as to strengthen the membrane between primary radial veins, wings of stick insect possess intercalary veins at the wing margin (**Fig. 3E**), a trait found in other orthopteroid insects. Here, we found two levels of intercalary veins (namely primary and secondary) in long wings with $L_w > 20$ mm, and only one level in short wings with $L_w < 20$ mm (**Fig. 3F**).

Overall, these trends indicate (i), a reorganization of primary radial veins (AA and PA) along the gradients of Q and p_w, and (ii) a loss of intercalary veins with decreasing L_w, which is coupled with conservation of inter-vein angle. Lastly, we highlight that, in forms with high wing loading, wings may

exhibit significant functional modification or loss of vein components, whereas those with relatively complete venation may preserve aerodynamic capacity (**Fig. 3F**).

3.3. Masses of wings and flight musculature

Among nine sampled species (Q between 0 – 0.8; L_w between 0 – 77 mm; L between 36 – 160 mm), the mass of a single wing (m_w) varied between 0.4 mg and 0.16 g. The scaling of wing mass with wing length was specific to each sex. For long wings with L_w > 5 cm, wing mass was about 0.1 g in both sexes. The scaling exponent of m_w was 2.2 and 1.2 in male and female insects, respectively (**Fig. 4A**). Correspondingly with reduced L_w, intersexual differences in m_w increased, with a lower m_w in wings of male insects.

Next, relative masses of both wings and flight musculature were positively correlated with relative wing size (Q), but not with body size (L) or wing loading (p_w) (**SI Table S1**), suggesting coupling with wing size at anatomical and developmental levels. The relative mass of wings (m_w') reached a maximum of 6% in the longest wings (Q = 0.8), and dropped to < 2% in short wings with Q < 0.4 (**Fig. 4B**). The power-law exponent of m_w' to Q in male insects was 0.1, which was twice that for female insects. The relative mass of flight muscle reached a maximum of 14% and also showed male-biased scaling, with male insects having a greater power-law exponent that was twice as large as that of the female insects (**Fig. 4C**).

We did not find an overall correlation between leg mass and wing size among all sampled insects. However, we found for the *A. tanarata* group that wing reduction was associated with increase in leg mass, possibly due to a tradeoff in energy allocation in the highland environment (see **SI Fig. S2B**).

3.4 Evolution of the body-leg system

Longitudinal mass distribution was fairly conserved in the two sexes, albeit with females having heavier abdomens. Using a two-section model for the body (**SI Fig. S1D**), the relative mass of the anterior body section (BS1) averaged 36.7% and 39.7% in females and males, respectively. The relative mass of posterior body section (BS2) averaged 48.2% and 33.5% in females and males, respectively. The relative mass of neither section was correlated with L, Q or p_w (see **SI Table S1**). Correspondingly, the longitudinal position of the center of mass (COM) was also conserved, lying at about 50% along the body length from the anterior end of head (hereafter abbreviated as 0.50 L; range 0.47 – 0.54 L) in females, and 0.44 L (range 0.41 – 0.46 L) in males, in both cases being generally located within 0.08 L near the median joint (**Fig. 5A**). The longitudinal positions of BS1, BS2 and COM were not correlated with L, Q, or p_w (see **SI Table S1**), except for a significant reduction in males of the mass of BS2 with increasing p_w. Wing mass was < 1% of body mass in all insects and had a negligible influence on the position of COM.

Total leg mass was generally conserved and not correlated with L, Q, or p_w. However, an increase in the relative mass of legs was correlated with body miniaturization in the *A. tanarata* group, suggesting a specific case of developmental tradeoffs (see **SI Section A**).

With increased wing loading, both the wing base and the median joint shifted from the anterior half of body to near the longitudinal center of body. The wing base, located at ~24% of body length L from the anterior end of head in insects with the lowest wing loadings, shifted posteriorly to ~0.40 L (**Fig. 5A**). The median joint also shifted posteriorly, from ~0.40 L to ~0.48 L in males, and from ~0.40 L to ~0.50 L in females. As both joints link to the metathoracic segment, these shifts resulted in a relative elongation of the mesothoracic segment and longitudinal compression of the abdominal section (**Fig. 5B**). Consequentially, distance between the wingbase and COM ($d_{wb\text{-}COM}$) was reduced to ~0.15 L in both sexes (**Fig. 5C**). Similarly, the distance from the median joint to COM was reduced to ~0.10 L in both sexes. The moment of inertia (MOI) of abdomen exhibited no significant variation with respect to wing

297 loading, despite the reduction of the BS2 mass in males (**Fig. 5D**). Lastly, the projected planform areas of
298 body and legs followed geometrical scaling and were only correlated with L, with power-law exponents
299 of ~2 (**Fig. 5E,F**).

300

301

4. Discussion

These results demonstrate systematic morphological reorganization of the flight apparatus and body plan during evolutionary loss of flight capacity in phasmids. Whereas a variety of selective scenarios may underlie such changes, we can identify the principal intercorrelations with respect to evolutionary changes in wing loading (**Fig. 6**). Wing morphology (e.g., wing shape and venation) exhibited stepwise variation in accordance with a critical wing loading value of ~10 Nm^{-2}, whereas most other morphological features were either significantly correlated with p_w and Q, or were predominately predicted by allometric scaling with body length.

4.1 Structural reconfiguration in partial wings

Considering variation in phasmid wing shape with respect to wing loading (**Fig. 2**), the aspect ratio (AR) range of 1.2 – 2.6 was somewhat low compared that in other flying insects (1.5 – 5.8; Bhat et al., 2019) but probably exceeds other clades in variability. In male stick insects, the positively correlation between AR and wing length L_w is likely an adaptation for enhanced aerodynamic efficiency (Kruyt et al., 2015), in accordance with the interpretation that male stick insects are under selection for dispersal capability (Zeng et al., 2020). In female stick insects, the reduction of wing AR with from low to medium-high p_w may indicate selection for non-flapping aerodynamic functions. Considering that these wings are used in various gliding behaviors (pers. obs., YZ), a low AR wing may help in drag production at high angles of attack (Ennos, 1989; Torres and Muller, 2004; Sunata et al., 2002). Why was this reduction only found in female insects? Females have a more posterior COM, and low AR wings may result in a more posterior center of aerodynamic pressure, reducing the static margin for stability (see below). Also, females are heavier than males and may have a greater demand for vertical force generation when parachuting or gliding. With little known about aerodynamics of such partial wings with low AR and operating at high p_w, kinematic data (e.g., flow fields, wing flapping kinematics, and wing deformation) along with force analysis would be necessary to further address functional significance of these differences.

In contrast to the wings of close relatives such as orthopteran and mantodean insects (Smart, 1953; Herbert et al., 2000), phasmid wings feature a narrow, elytrized costal edge that covers their slender abdomen, and the radially organized veins support the majority of wing membrane, allowing it to fold in fanlike fashion. The variation in the radial veins follows two trends: (1) stepwise reduction of functional modules along with the gradient in Q and p_w, and (2) loss of hierarchical levels with reducing wing size L_w (**Fig. 3F**).

At the whole-wing level, reduction of the number of veins with decreasing Q is likely a case of truncated development. For the AA veins, which are directly associated with wing depressor muscles (**SI Fig. S1C**), reduction at medium-high p_w is likely coupled with a reduction in downstroke capability. The PP veins appear as a modularized component, which contributes to a large part of the variation in vein number and wing area (**Fig. 3A**). This variability in number may be regulated as developmental duplication, and could contribute to relatively rapid evolution of wing gain or reduction in phasmids (Zeng et al., 2020; Bank and Bradler, 2022). Although not analyzed here, miniaturized wings of $Q < 0.3$ seem to possess high variability in design and functionality (**Fig. 3F**). Over this high-p_w regime, maintenance of the complete wing membrane (such as in At3f and At3m; **SI Fig. S3A**) suggests reduced yet non-trivial aerodynamic utility.

Lastly, both wing shape and venation of partial wings may contribute to wing deformation (e.g., camber formation) during aerial descent (pers. obs., YZ). For the next step, analysis of wing flapping kinematics is necessary to address the function of different vein groups, and to biomechanically understand phasmid wing evolution.

4.2 Scaling of wing inertia and flight muscle

The positive correlation of wing mass with wing size shows that wings are not isometrically condensed as their size is reduced, or that less cuticle is put into their construction. With mean scaling exponents of 1.2 and 2.2 (**Fig. 4A**), wing mass scaling lies in between simple models assuming uniform thickness (exponent of 1) and isometric scaling (exponent of 3), suggesting that thickness increases along with wing size. Convergence of mass in long wings from both sexes (**Fig. 4B**) is in accordance with the high AR of long wings in both sexes. For shorter wings, those of female insects had greater mass (**Fig. 4A**), which may be associated with wider elytrized costal edges (**SI Fig. S3**). At the whole-insect level, relative masses of wings and flight musculature can be reliably predicted using Q (**Fig. 4B,C**).

Male insects had relatively greater wing and flight muscle, with the wings representing ~6% of whole-insect mass. Also, linear reduction in the relative mass of flight muscle suggests a close coupling with wing size. Reduction in flight muscle mass may be associated with loss and reconfiguration of different muscle groups, as well as with an overall reduction in wing flapping capability. Together, these data suggest a reduction of wing inertia and flapping capability as Q decreases, which predicts less effective force production during flapping.

4.3 Changes in the body-leg system during flight loss

For the body-leg system, only the longitudinal positions of pterothoracic segments and associated joints exhibited significant variation with respect to p_w and Q. The p_w-invariant parameters (including COM position, masses of BS1 and legs, and projected planform area of body and legs) were conserved and followed near-isometric scaling. This result suggests limited influence of selection on flight-related functions; however, aerodynamic and inertial roles of legs and abdomen can be directly regulated via movements and postural control in flight. The role of body-leg postural control in flight performed with variously sized wings could be addressed in future research.

The posterior shift of pterothoracic segments may help to maintain stability during descending flights performed with partial wings. Passively stable aerodynamic configurations are achieved through the moment balance between forces produced on wings and on the body-leg system (Zeng et al. 2017). Critical for such a configuration is a statically stable posture of the insect (including wings and body-leg sections) with the center of pressure located vertically above the COM (if vertically parachuting), or posterior to the COM (if gliding with a forward component of velocity). In both cases, partial wings would generate vertical forces with reduced or no flapping. Also, the demand for abdominal oscillation (**SI Fig. S1D**) is likely reduced or lost altogether as flight diminishes, because wing motions are either not oscillatory or are doing so only in small amplitude.

The posteriorward shift of the pterothorax and a corresponding reduction in wingbase-COM distance (**Fig. 5A-C**) can effectively reduce the magnitude of wing-induced moments, compensating for instability induced by wing forces. It may also shift the aerodynamic center more posteriorly and reduce the static margin (which is negative when the center of pressure is posterior to the COM), yielding better passive stability. In the direction of flight gain, a positive static margin may be necessary for flapping flight in fully-winged insects. So far, kinematics of wing flapping and flight performance have only been documented in a leaf insect (Boisseau et al., 2022). These predictions need to be confirmed using actual body-leg postures and body kinematics, along with stability analysis, from flight of phasmids with various sized wings.

References

Abràmoff, M. D., Magalhães, P. J. and Ram, S. (2004). Image processing with ImageJ. *Biophotonics international* **11**, 36-43.

Boisseau, R. P., Büscher, T. H., Klawitter, L. J., Gorb, S. N., Emlen, D. J. and Tobalske, B. W. (2022). Multi-modal locomotor costs favor smaller males in a sexually dimorphic leaf-mimicking insect. *BMC Ecology and Evolution* **22**, 1-18.

Bragg, P. E. (1997). A glossary of terms used to describe phasmids. *Phasmid Studies* **6**, 24-33.

Brock, P. D. (1999). *Stick and leaf insects of Peninsular Malaysia and Singapore*, Malaysian Nature Society.

Dudley, R. (2000). *The biomechanics of insect flight: form, function, evolution*, Princeton Univ Pr.

Dudley, R., Byrnes, G., Yanoviak, S. P., Borrell, B., Brown, R. M. and McGuire, J. A. (2007). Gliding and the Functional Origins of Flight: Biomechanical Novelty or Necessity? *Annual Review of Ecology, Evolution, and Systematics* **38**, 179-201.

Dudley, R. and Yanoviak, S. P. (2011). Animal aloft: the origins of aerial behavior and flight. *Integr Comp Biol* **51**, 926-936.

Ellington, C. P. (1991). Aerodynamics and the origin of insect flight. *Adv. Insect Physiol* **23**, 171-210.

Ennos, A. R. (1989). The effect of size on the optimal shapes of gliding insects and seeds. *Journal of Zoology* **219**, 61-69.

Herbert, R. C., Young, P. G., Smith, C. W., Wootton, R. J. and Evans, K. E. (2000). The hind wing of the desert locust (*Schistocerca gregaria* Forskal). III. A finite element analysis of a deployable structure. *Journal of Experimental Biology* **203**, 2945-2955.

Kruyt, J. W., Van Heijst, G. F., Altshuler, D. L. and Lentink, D. (2015). Power reduction and the radial limit of stall delay in revolving wings of different aspect ratio. *Journal of the Royal Society Interface* **12**, 20150051.

Kukalová-Peck, J. (1983). Origin of the insect wing and wing articulation from the arthropodan leg. *Can J Zool* **61**, 1618-1669.

Le Roy, C., Debat, V. and Llaurens, V. (2019). Adaptive evolution of butterfly wing shape: from morphology to behaviour. *Biological Reviews* **94**, 1261-1281.

Mani, M. S. (2013). *Ecology and biogeography of high altitude insects*, Springer Science & Business Media.

Marden, J. H. (2003). The surface-skimming hypothesis for the evolution of insect flight. *Acta zoologica cracoviensia* **46**, 73-84.

Orme, D., Freckleton, R., Thomas, G. and Petzoldt, T. (2013). The caper package: comparative analysis of phylogenetics and evolution in R. *R package version* **5**, 1-36.

Paradis, E., Claude, J. and Strimmer, K. (2004). APE: analyses of phylogenetics and evolution in R language. *Bioinformatics* **20**, 289-290.

Perrard, A., Baylac, M., Carpenter, J. M. and Villemant, C. (2014). Evolution of wing shape in hornets: why is the wing venation efficient for species identification? *Journal of Evolutionary Biology* **27**, 2665-2675.

Ragge, D. R. (1955). The wing-venation of the order Phasmida. *Transactions of the Royal entomological Society of London* **106**, 375-392.

Ritz, C., Baty, F., Streibig, J. C. and Gerhard, D. (2015). Dose-Response Analysis Using R. *PLoS One* **10**.

Roff, D. A. (1994). The evolution of flightlessness: is history important? *Evolutionary Ecology* **8**, 639-657.

Seow-Choen, F. (2000). *An illustrated guide to the stick and leaf insects of Peninsular Malaysia and Singapore*, Natural History Publications (Borneo).

Smart, J. (1953). The wing-venation of the migratory locust (Locusta migratoria Linn.)(Insecta: Acridiidae). *Proceedings of the Zoological Society of London* **123**, 207-217.

Sunada, S., Yasuda, T., Yasuda, K. and Kawachi, K. (2002). Comparison of wing characteristics at an ultralow Reynolds number. *Journal of aircraft* **39**, 331-338.

Thomas, A. L. and Taylor, G. K. (2001). Animal flight dynamics I. Stability in gliding flight. *J Theor Biol* **212**, 399-424.

Torres, G. E. and Mueller, T. J. (2004). Low-aspect-ratio wing aerodynamics at low Reynolds number. *AIAA Journal* **42**, 865-873.

Zeng, Y., Lam, K., Chen, Y., Gong, M., Xu, Z. and Dudley, R. (2017). Biomechanics of aerial righting in wingless nymphal stick insects. *Interface Focus* **7**, 20160075.

Zeng, Y., O'Malley, C., Singhal, S., Rahim, F., Park, S., Chen, X. and Dudley, R. (2020). A tale of winglets: evolution of flight morphology in stick insects. *Frontiers in Ecology and Evolution* **8**, 121.

Main Figures

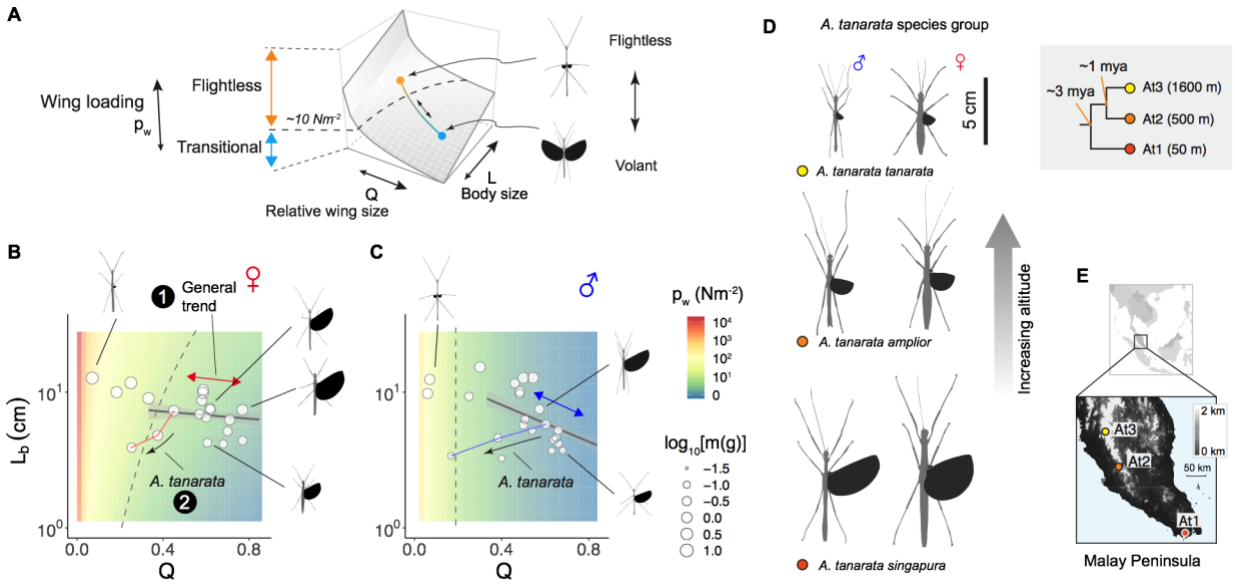

Figure 1. General patterns of flight-related morphology in stick insects.

(A) Evolution of flight morphology in stick insects can be represented by trajectories on a landscape of wing loading (p_w) defined by relative wing size (Q) and body size (L) (see Zeng et al., 2020). Stick insects exhibit a continuous transition from flight-capable to flightless morphology over p_w < ~10 Nm^{-2}

(B) Male and **(C)** female stick insects sampled here and plotted on sex-specific p_w landscapes, with dashed contour lines showing critical p_w ~ 10 Nm^{-2}, with dot size representing whole-insect mass. Solid trend lines represent the general pattern – an inverse correlation between L and Q in flight evolution (based on ~270 morphologies for each sex; see Zeng et al., 2020). As an outlier, the *Asceles tanarata* species group (annotated with arrows) exhibited intraspecific reductions in both L and Q with increasing altitude.

(D) Dorsally projected profiles of the three subspecies of the *A. tanarata* species group, showing reductions in body and wing size at greater altitude. At right are the phylogenetic relationships among three subspecies, with nodes annotated with divergence time (see Zeng et al., 2020).

(E) An altitudinal map of the Malay Peninsula, annotated with locations where three subspecies were collected: At1, Singapore; At2, Cameron Highland; At3, Genting Highland.

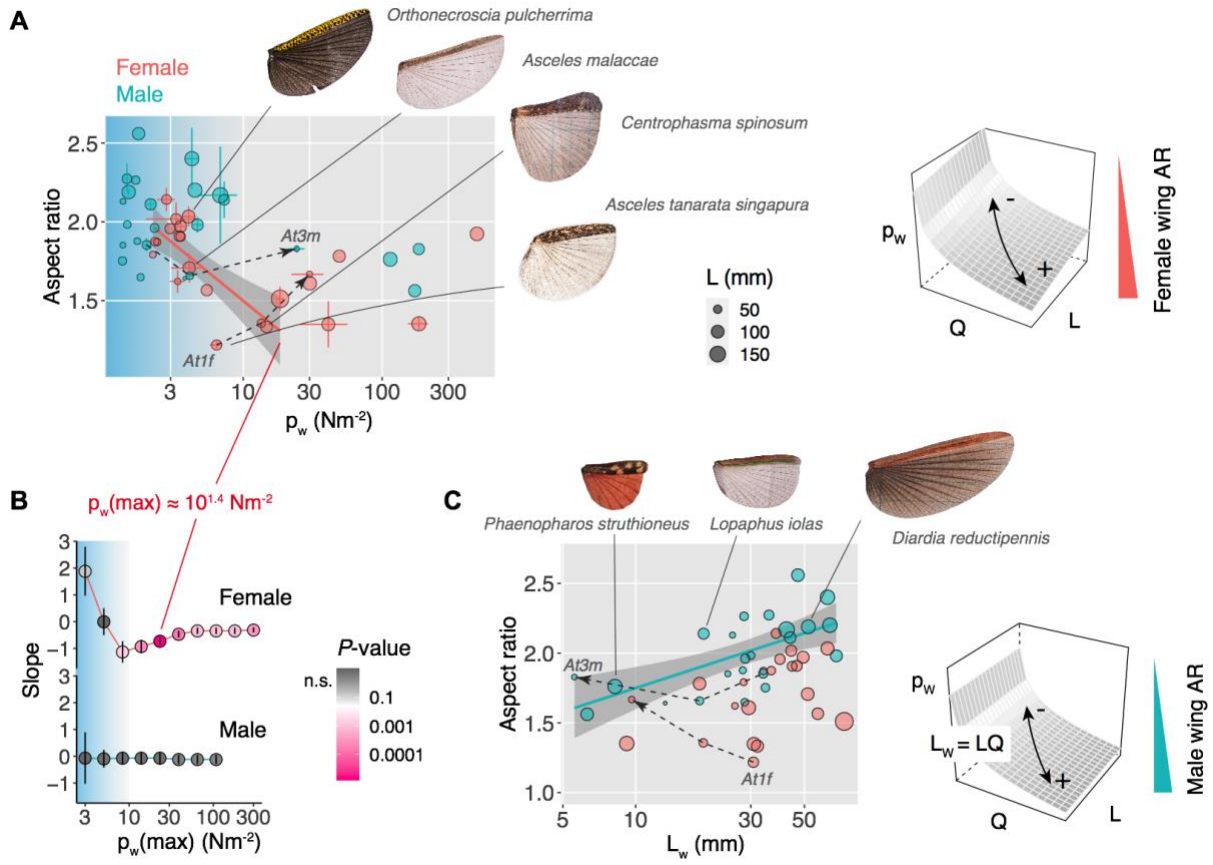

Figure 2. Sex-specific evolution of stick insect wing shape.

(A) Wing aspect ratio (AR) versus wing loading (p_w) (N = 25 for both female and male taxa). Colors represent sexes; dot sizes represent body length. Note a clear reduction of AR in wings of females over $p_w > 4$ Nm^{-2}, while wings of male insects show no such reduction. Such trend is further elucidated with a sensitivity analysis in **(B)**, where generalized linear regression models were performed with different upper limit of wing loading, p_w(max). The variation of slope coefficient was plotted against p_w, with error bars representing standard error, and color representing P-value. For females, the lowest slope coefficient corresponds with p_w(max) = $10^{0.92}$ Nm^{-2}, while the lowest P-value corresponds with p_w(max) = $10^{1.4}$ Nm^{-2}, as shown by the trend line in (A). For males, the correlation between AR and p_w was non-significant and insensitive to the choice of p_w(max).

(C) The variation of AR with absolute wing length (L_w = LQ), whereby the wings of males exhibited a significant positive correlation ($P < 0.01$) with increasing L_w. Annotated at the right are schematics summarizing sex-specific variation in wing shape: the AR in females varies with p_w, while the AR in males correlates with L_w, thus varying with body size L despite the p_w landscape being invariant of body size (see Zeng et al., 2020). In **(A)** and **(C)**, arrows with dashed lines represent variation within *A. tanarata* species group along increasing altitude. See **SI Data S2** for phylogenetically justified correlations.

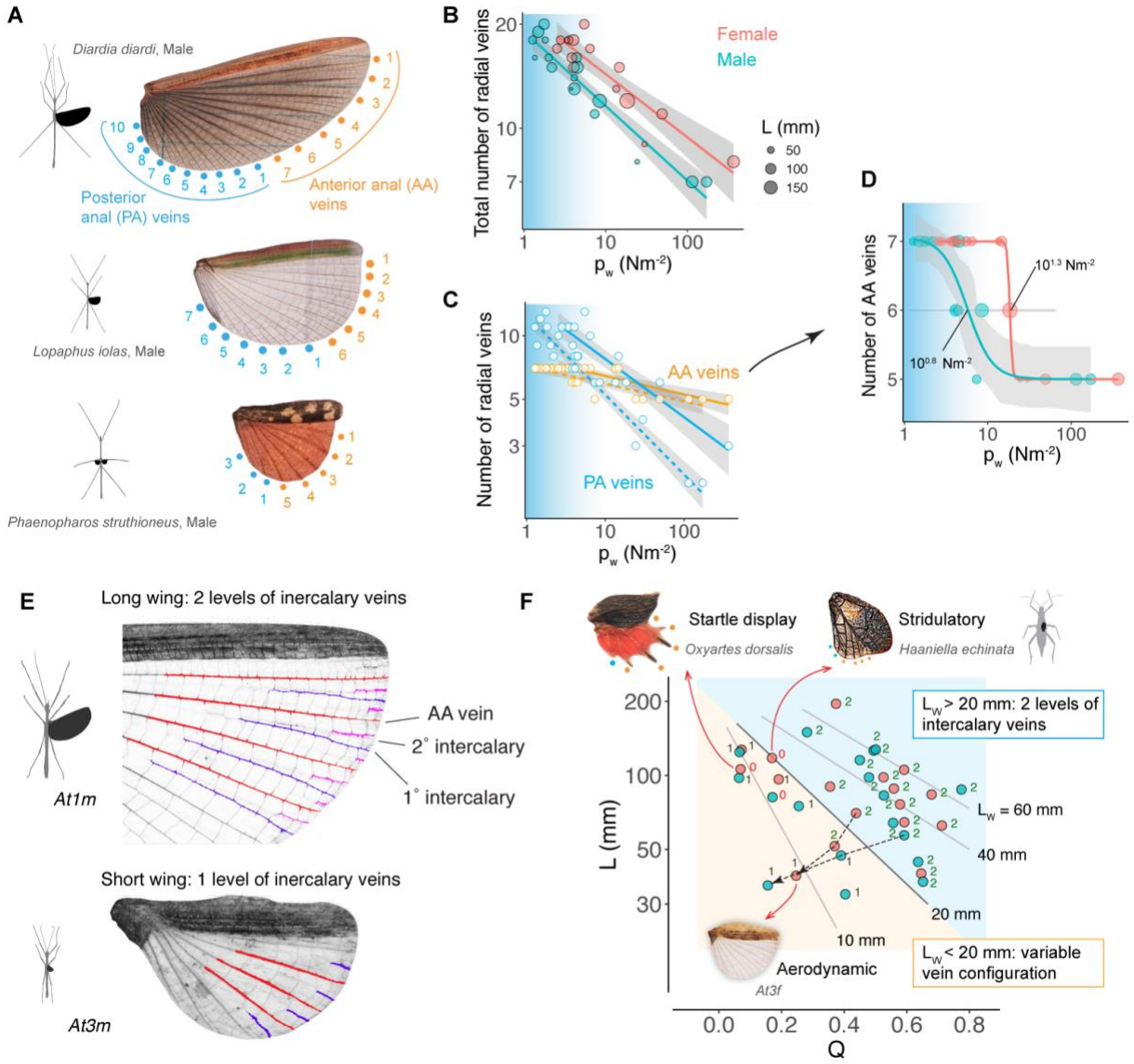

Figure 3. Evolution of stick insect wing venation.

(A) Exemplar wings showing reduction of primary radial veins – anterior anal (AA) and posterior anal (PA) veins. The number of AA veins is conserved, while the number of PA veins varies with relative wing size and wing loading. **(B)** The total number of radial veins (N_V) reduces with increasing wing loading p_w (N = 34 female taxa; N = 36 male taxa). **(C)** Considering two vein groups individually, the number of PA veins varied between 2 – 14 (blue) and is linearly correlated with p_w, while the number of AA veins (N_{AA}) is more conserved, varying between 5 – 7 (orange). Trend lines are based on linear regression models.

(D) The transition of N_{AA} from 7 to 5 with increasing p_w, as fitted with sigmoid functions (**SI Data S1**). The model-predicted critical p_w at N_{AA} = 6 is $10^{0.75}$ Nm^{-2} and $10^{1.3}$ for males and females, respectively.

(E) As gap size between adjacent radial veins increases toward the wing margin, intercalary veins are developed. Long wings possess two levels of intercalary veins, while short wings possess only one, as demonstrated here using At1m and At3m. **(F)** Across all sample taxa, the loss of the 2˚ intercalary vein corresponds with absolute wing length L_w < ~20 mm. Plot shows the levels of intercalary veins as numbers with respect to L and Q, where isolines represent L_w. Relatively more variable venation with derived functions was found in the regime of L_w < 20 mm. Two wings with non-aerodynamic functions and no intercalary veins are annotated on the top, contrasting another wing (from At3f) with 1˚ intercalary veins and potential aerodynamic utility. Values correspond to taxa-specific means; in **(B)**, **(D)** and **(F)**, dashed lines with arrows show variation in the *A. tanarata* group.

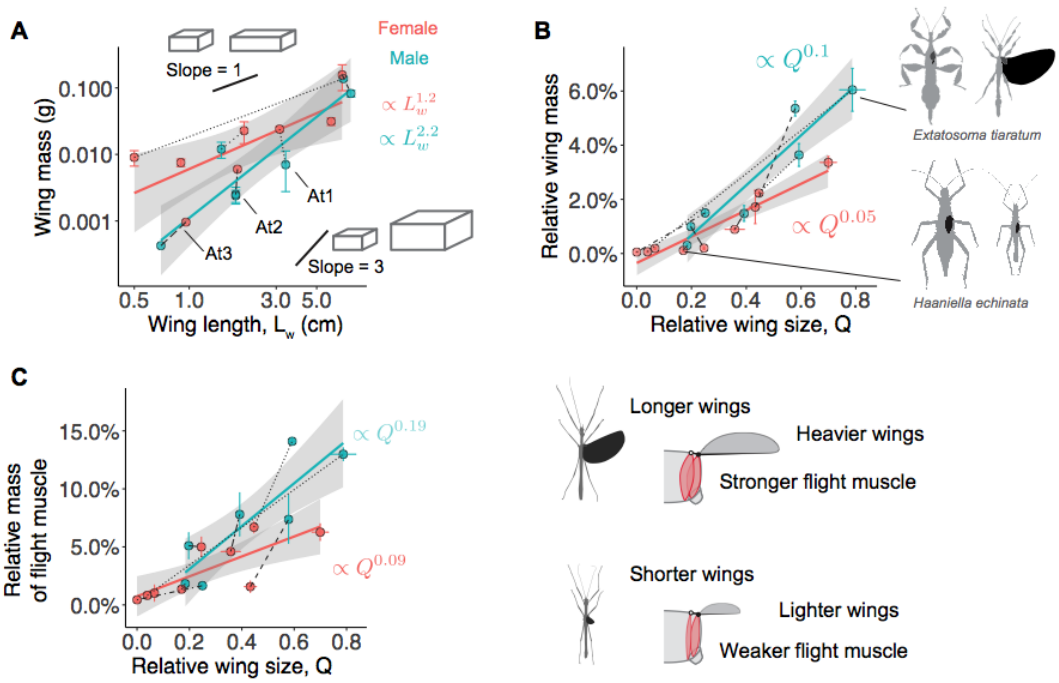

Figure 4. Scaling of wing mass and flight muscle mass.

(A) Sex-specific scaling of wing mass with respect to absolute wing length (L_w) (*N* = 9 female taxa; *N* = 7 male taxa). Point shape and trend lines represent different sexes; colors represent different species. Females possess heavier wings than males with the same wing size. The power-law exponents (1.2 – 2.2) are intermediate to two models: (i) exponent = 3, if dimensions of wings increase isometrically in all three dimensions; (ii) exponent = 1, if wing thickness were conserved and mass is proportional to wing length.

(B) The power-law scaling of relative wing mass (i.e., with respect to whole-insect mass) with respect to relative wing size Q, showing that females possess relatively lighter wings than males.

(C) The power-law scaling of flight muscle mass with respect to relative wing size Q, showing that males have greater volume of flight muscle than females. Values represent taxa-specific means±S.D. Trend lines are based on linear regression models; males and females of the same species are connected by dashed or dotted lines.

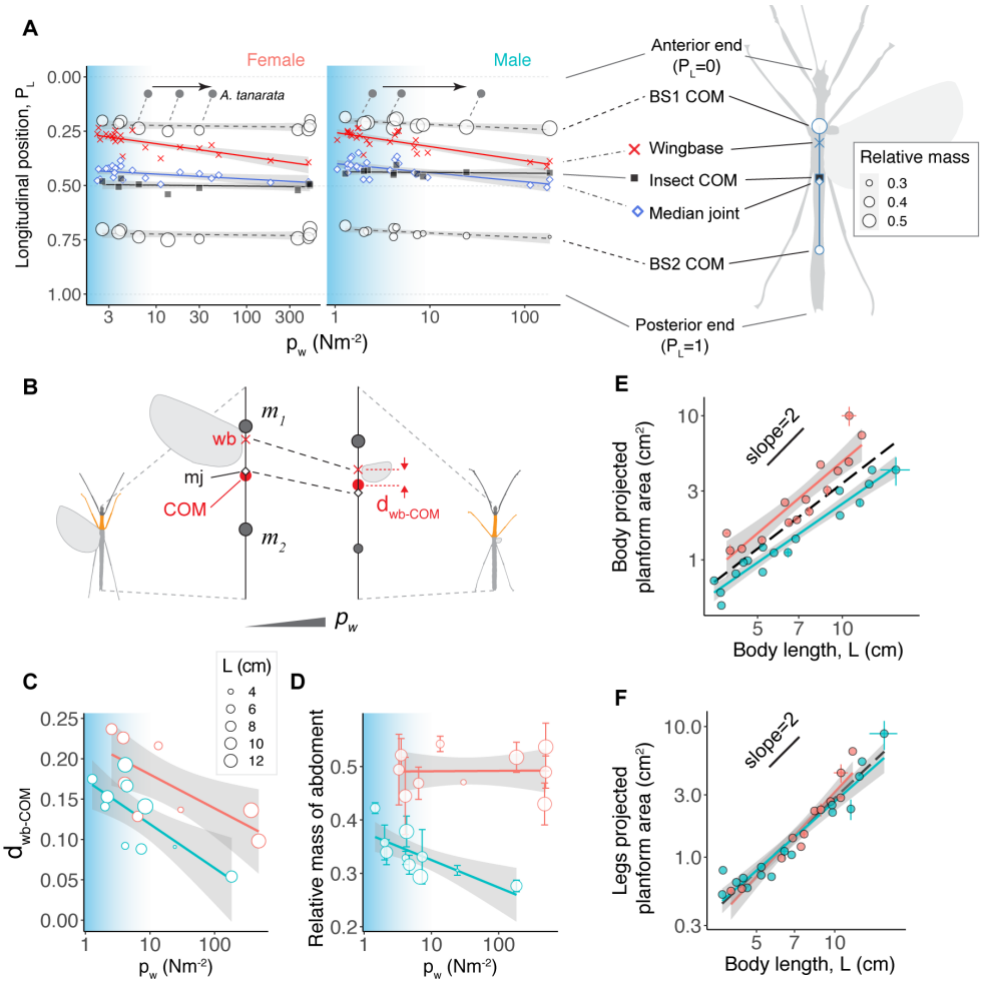

Figure 5. Variations of body and leg morphology.

(A) Normalized longitudinal positions of flight-related morphological landmarks plotted against wing loading (p_w) (see legend to the right). The positions of the wingbase (red) and median joint (blue) shift posteriorly with increasing p_w, while the position of whole-insect COM is relatively unchanged. The size of open dots represents relative mass (N = 10 for both male and female taxa); trend lines are based on linear regression models (N = 23 female taxa; N = 26 male taxa). Black arrows represent the *A. tanarata* species group along increasing altitude. **(B)** Schematic demonstration of shifts in wingbase (wb) and median joint (mj) with respect to wing reduction, which is coupled with elongation of the mesothoracic segment (orange), as demonstrated with two exemplar profiles.

(C) The distance between wingbase and whole-insect COM ($d_{wb\text{-}COM}$) decreases with increasing p_w in both sexes. **(D)** The relative mass of abdomen decreases with increasing p_w in males, but not in females.

(E) Projected planform area of body sections scales with body size with a sex-averaged power-law exponent 1.54 ± 0.15 (mean ± S.E.) (N = 18 female taxa; N = 20 male taxa). An exponent < 2 suggests disproportionate increase in slenderness as stick insects become longer. The greater slope intercept in females corresponds to wider body segments. **(F)** Projected planform area of all legs exhibits a near-isometry with body length, with a sex-averaged power-law exponent of 1.74 ± 0.13 (mean ± S.E.). See **SI Table S1** and **Data S1** for details.

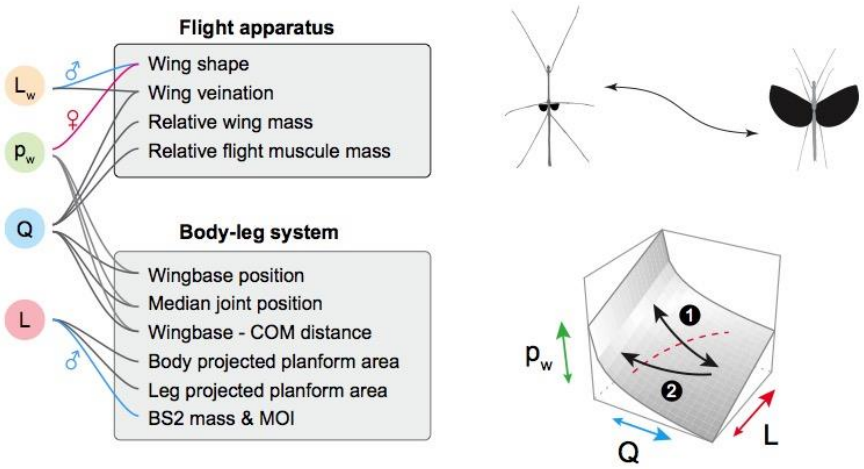

Figure 6. Summary of the evolution of flight-related morphology in stick insects.

(Left) Summary of correlations between morphological and flight-relevant parameters for four principal variables (wing loading, p_w; relative wing size, Q; body size, L; absolute wing size L_w). Colored lines represent sex-specific correlations. See **SI Table S1** for more details.

(Right) Two types of evolutionary trajectories on the p_w landscape in phasmids: (1) the general inverse correlation between L and Q, and (2) coupled reductions in L and Q exhibited by the *A. tanarata* species group (see **SI Section A** for more details). Gain and loss of flight (most generally represented by p_w) mainly follow the direction of wing size evolution (Q), but are influenced by body size evolution and other sex-specific traits within a variety of ecological contexts.

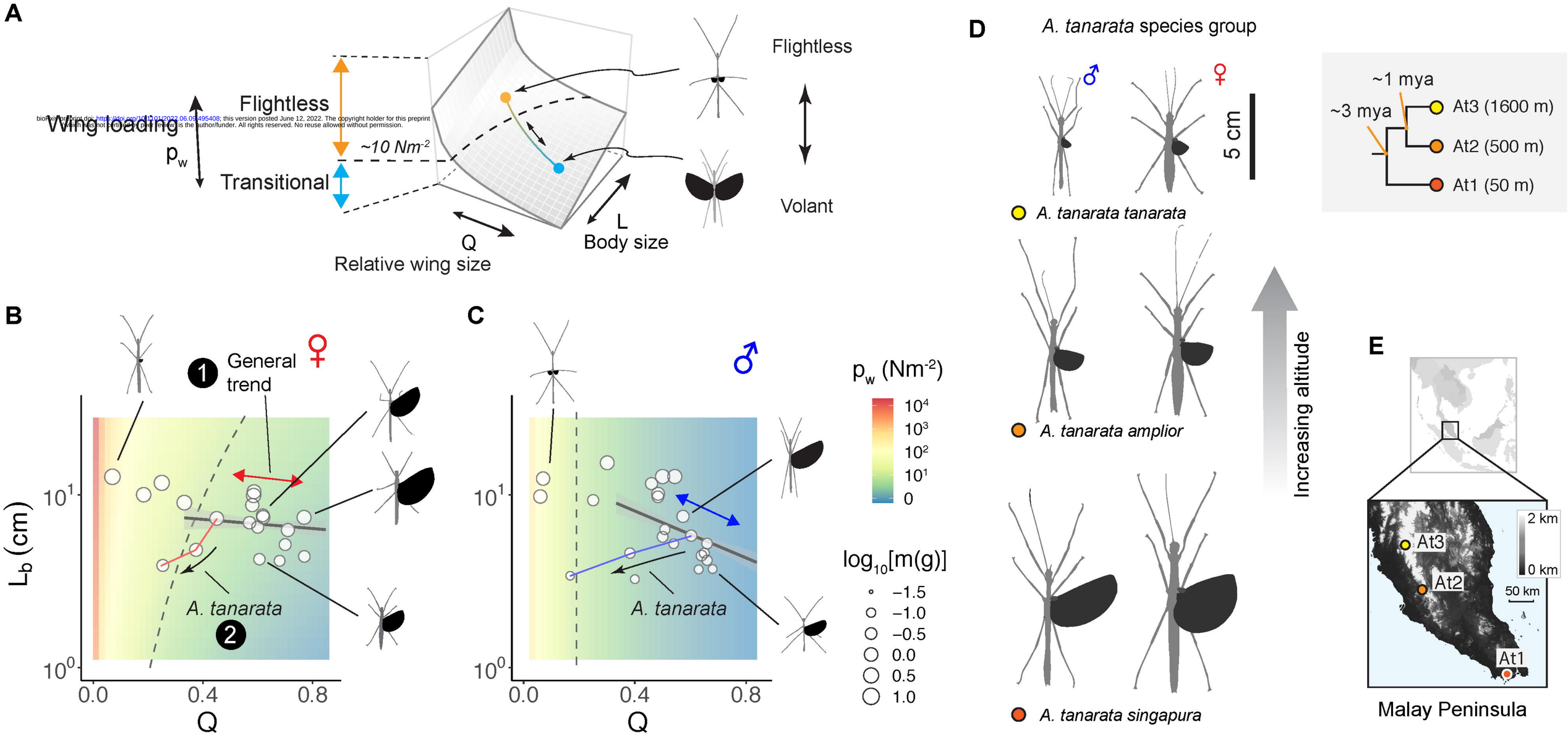

A

Orthonecroscia pulcherrima

Asceles malaccae

Centrophasma spinosum

Asceles tanarata singapura

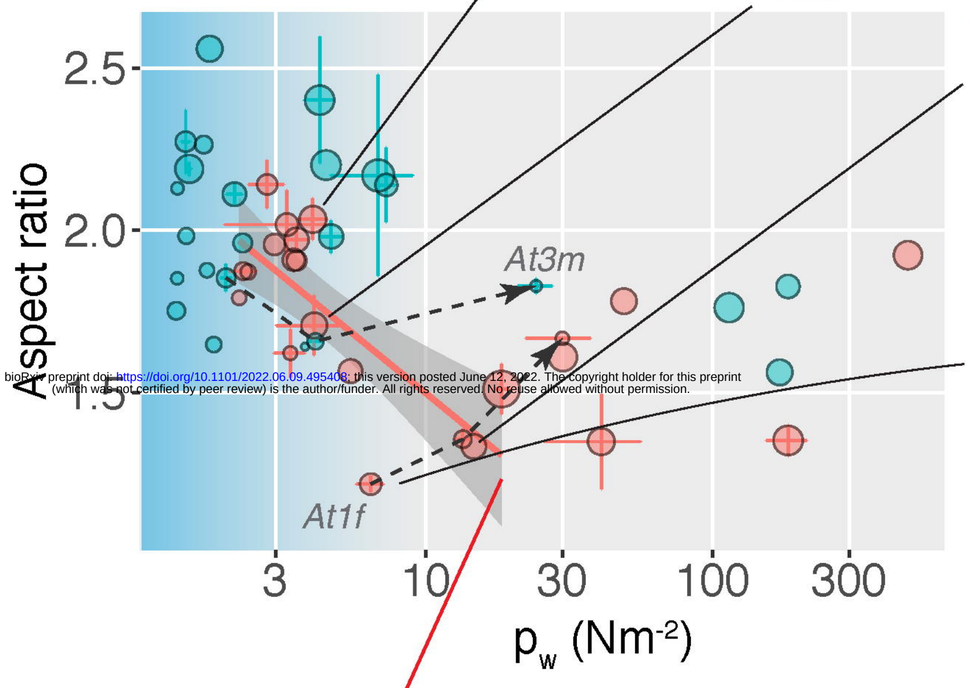

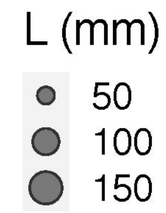

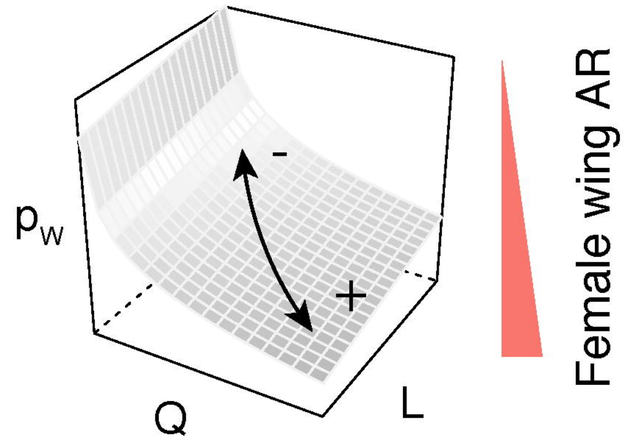

B

$p_w(max) \approx 10^{1.4}$ Nm^{-2}

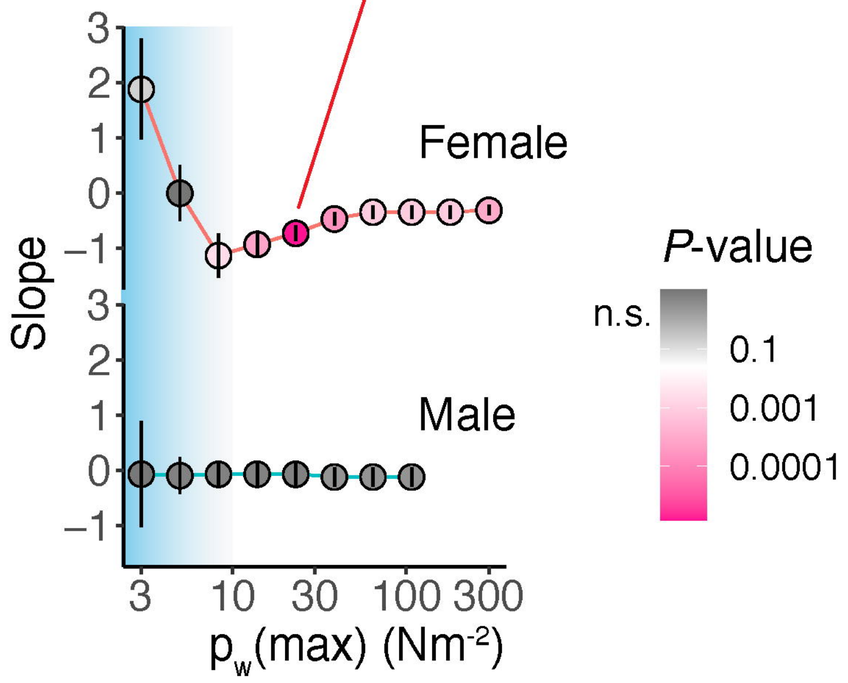

C

Phaenopharos struthioneus

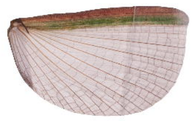

Lopaphus iolas

Diardia reductipennis

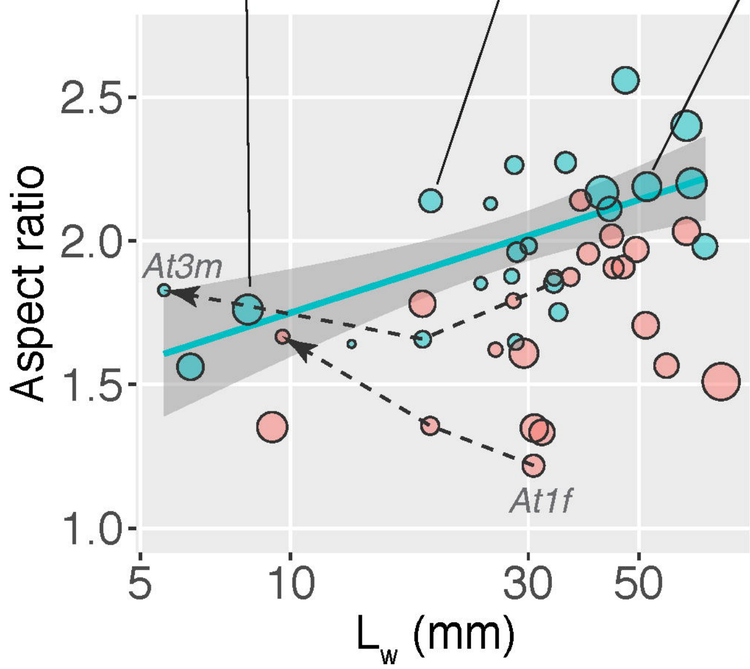

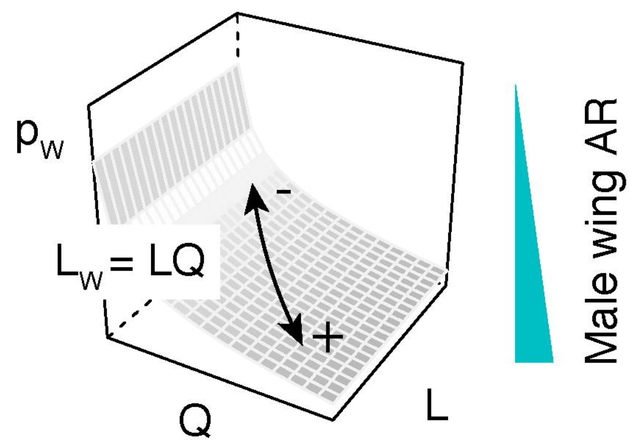

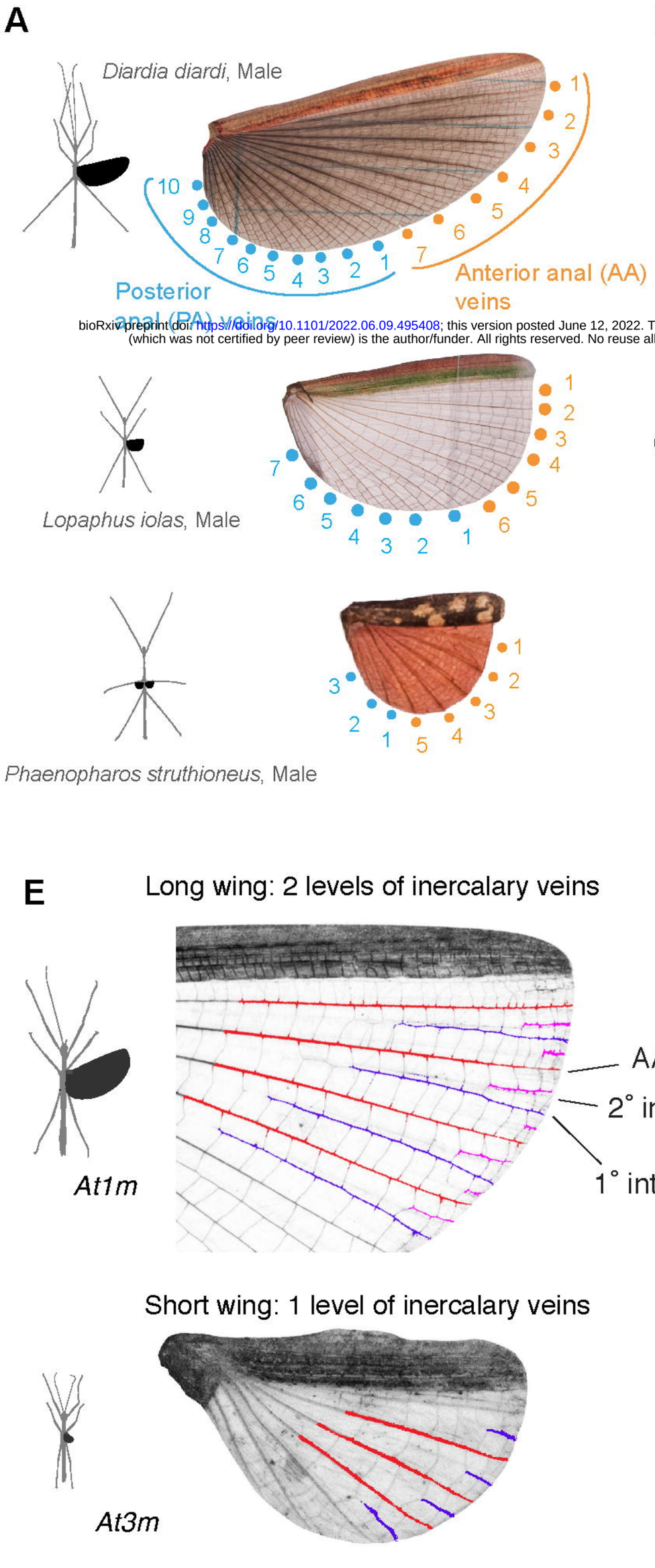

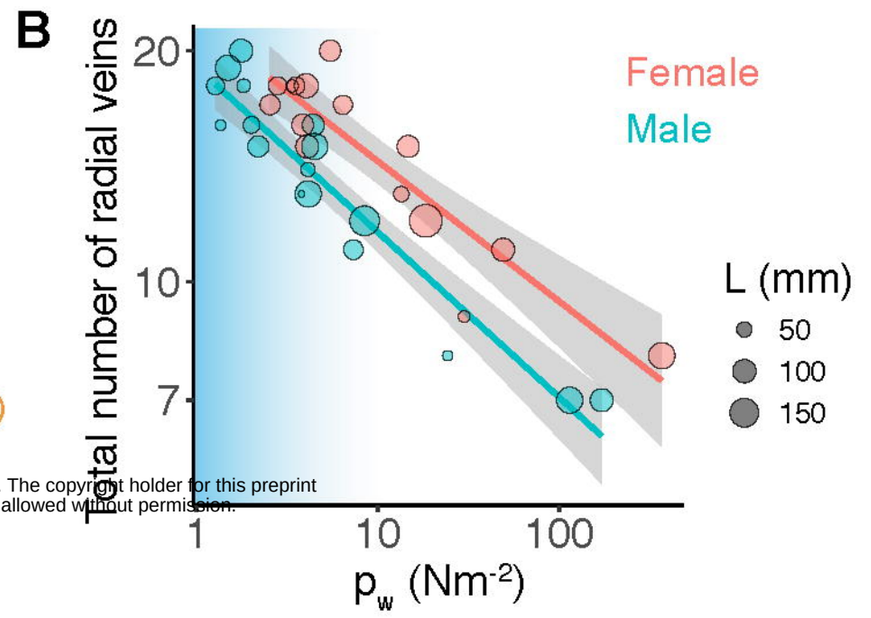

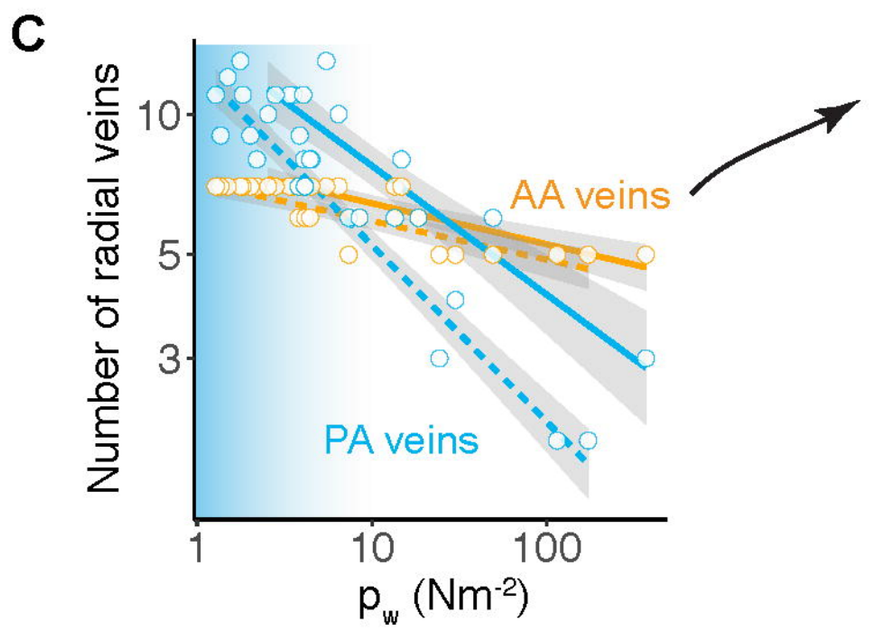

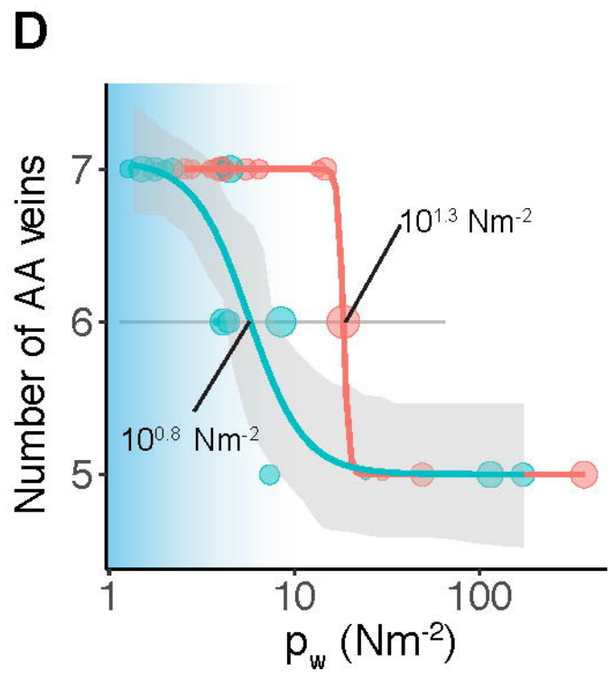

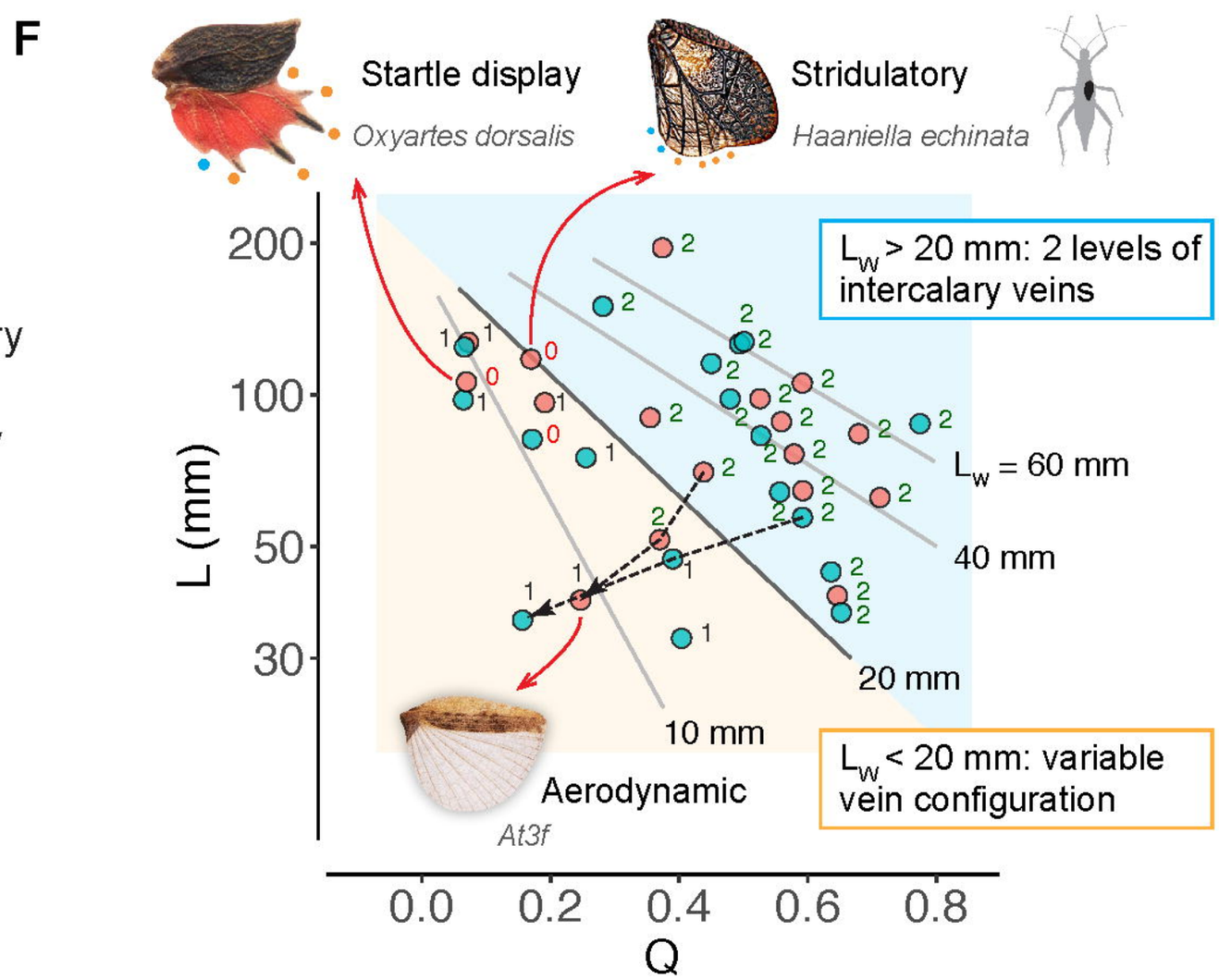

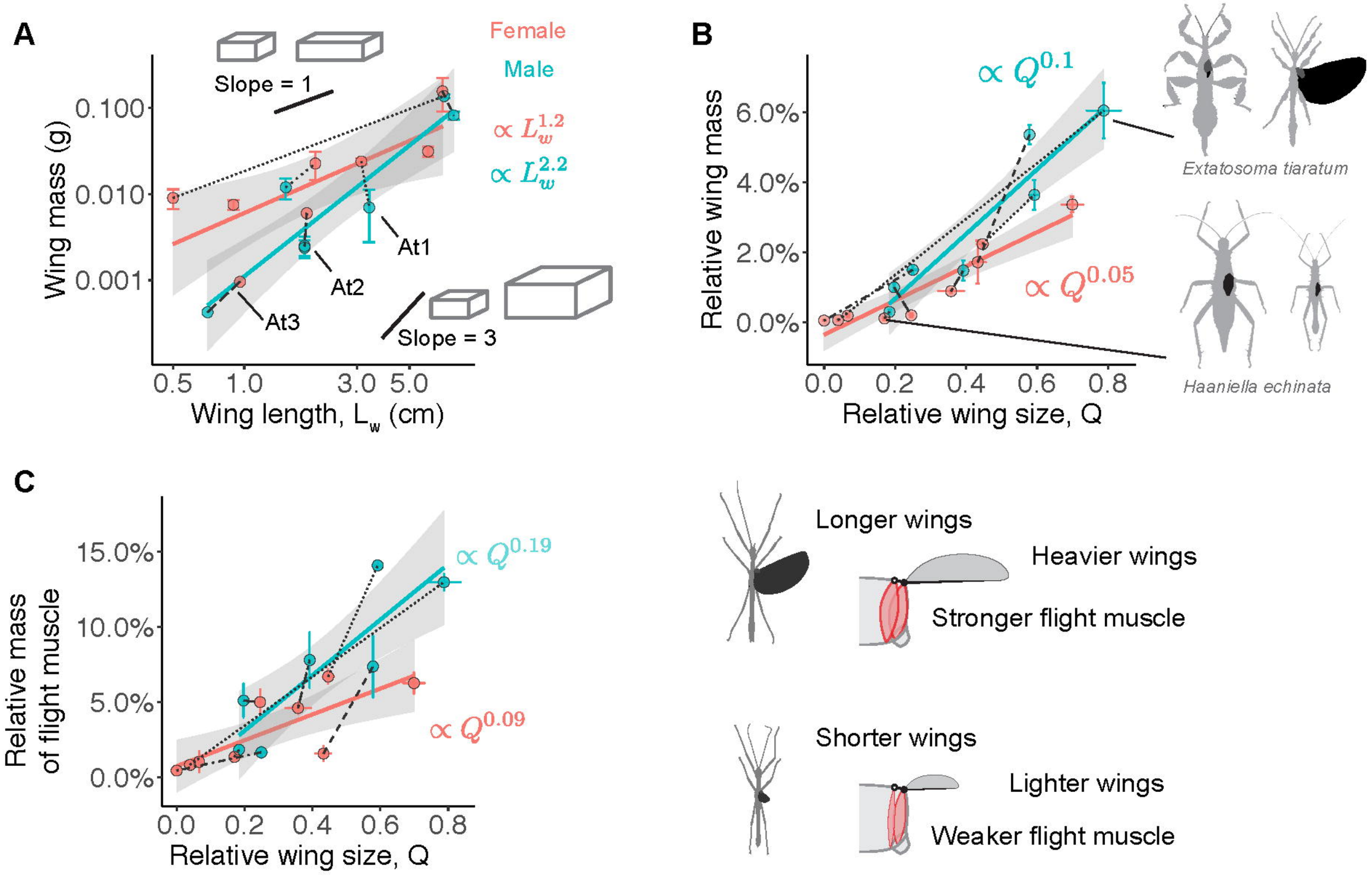
A
Female
Male
Slope = 1
$\propto L_w^{1.2}$
$\propto L_w^{2.2}$
At1
At2
At3
Slope = 3
Wing mass (g)
0.100
0.010
0.001
0.5
1.0
3.0
5.0
Wing length, L_w (cm)
B
$\propto Q^{0.1}$
$\propto Q^{0.05}$
Relative wing mass
6.0%
4.0%
2.0%
0.0%
0.0
0.2
0.4
0.6
0.8
Relative wing size, Q
Extatosoma tiaratum
Haaniella echinata
C
$\propto Q^{0.19}$
$\propto Q^{0.09}$
Relative mass of flight muscle
15.0%
10.0%
5.0%
0.0%
0.0
0.2
0.4
0.6
0.8
Relative wing size, Q
Longer wings
Heavier wings
Stronger flight muscle
Shorter wings
Lighter wings
Weaker flight muscle

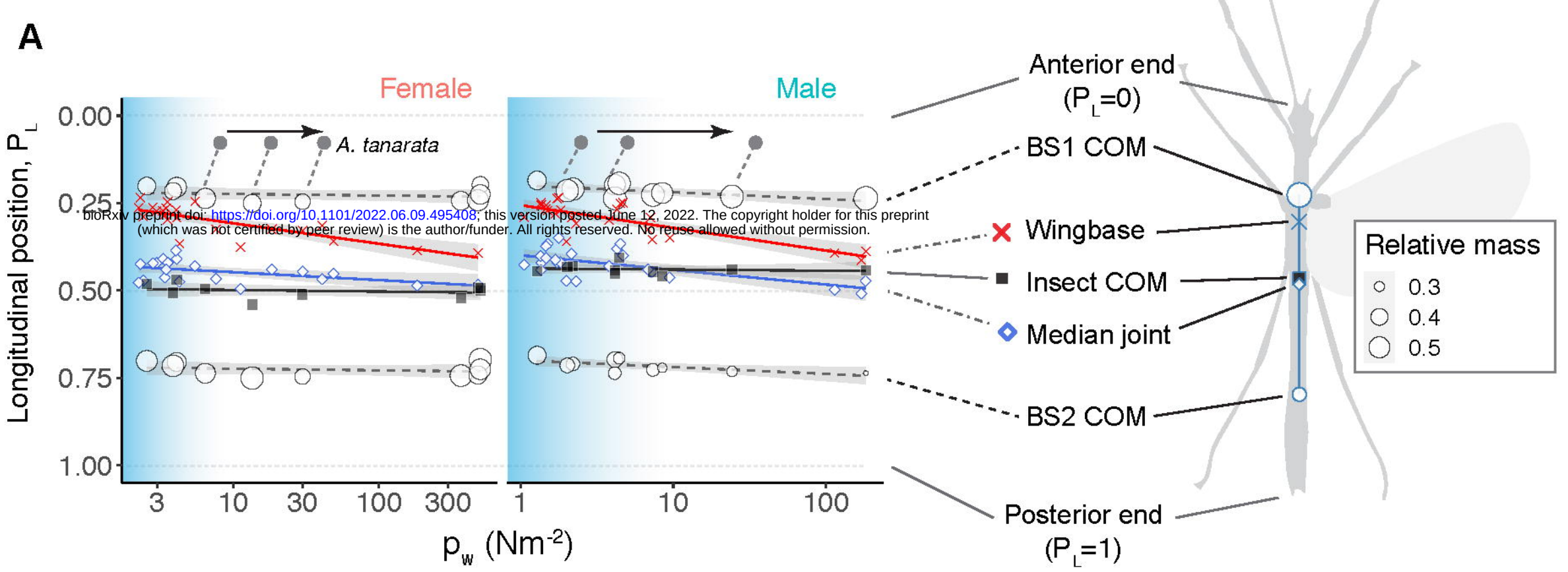

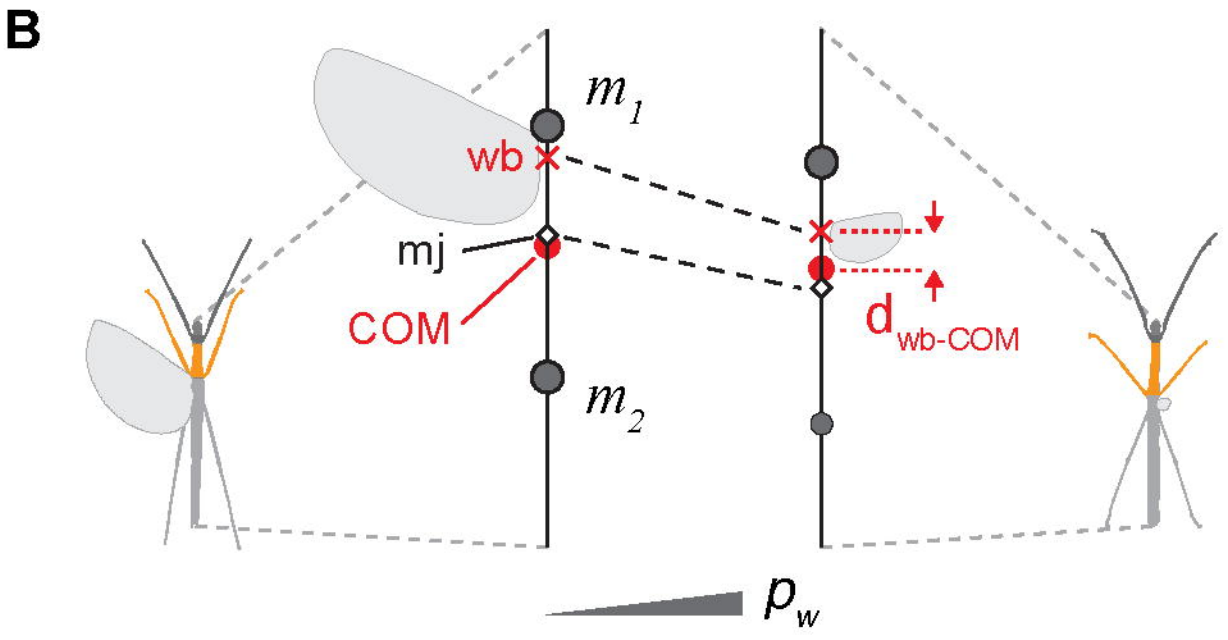

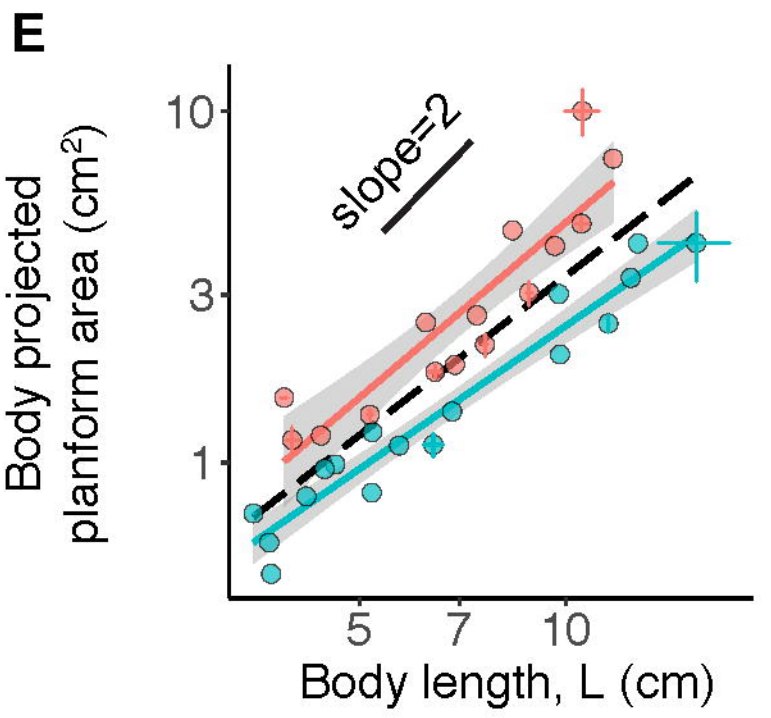

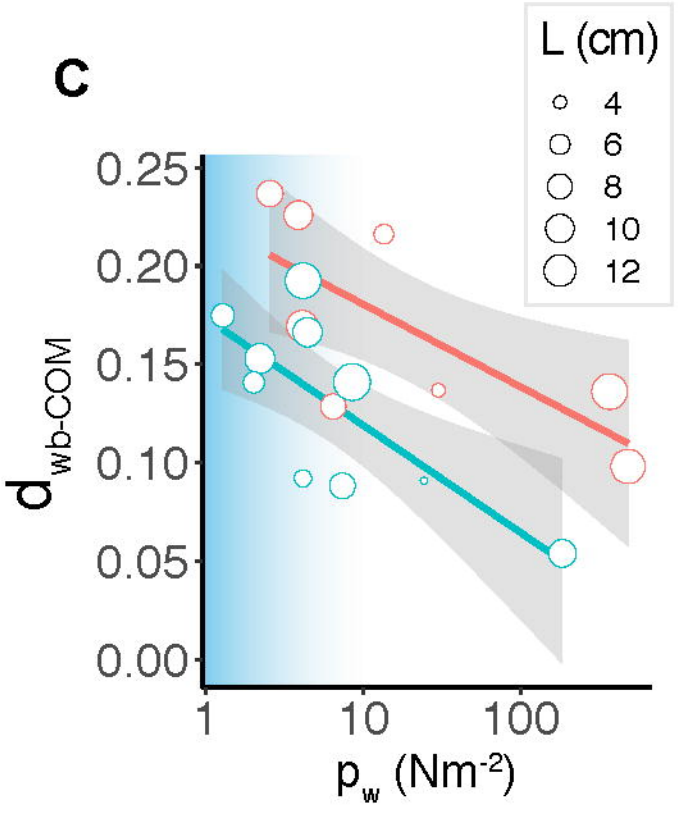

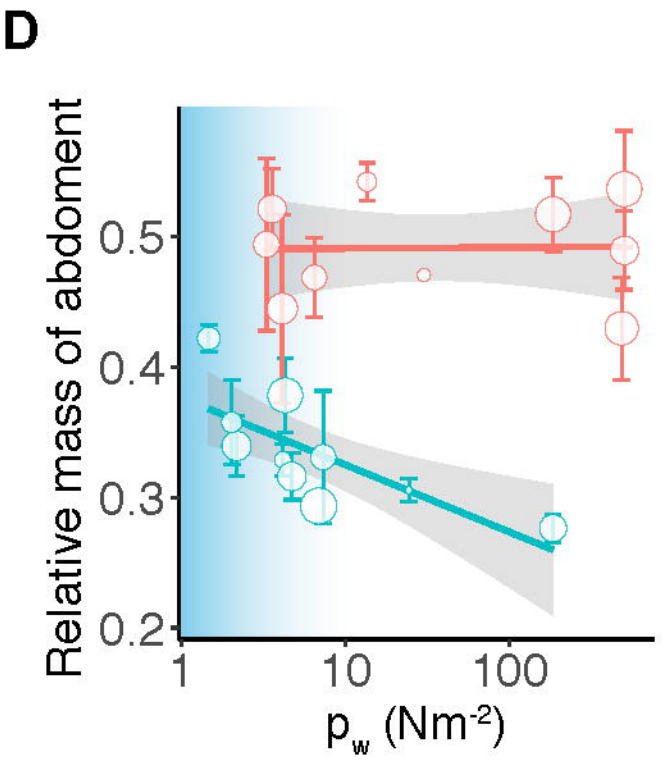

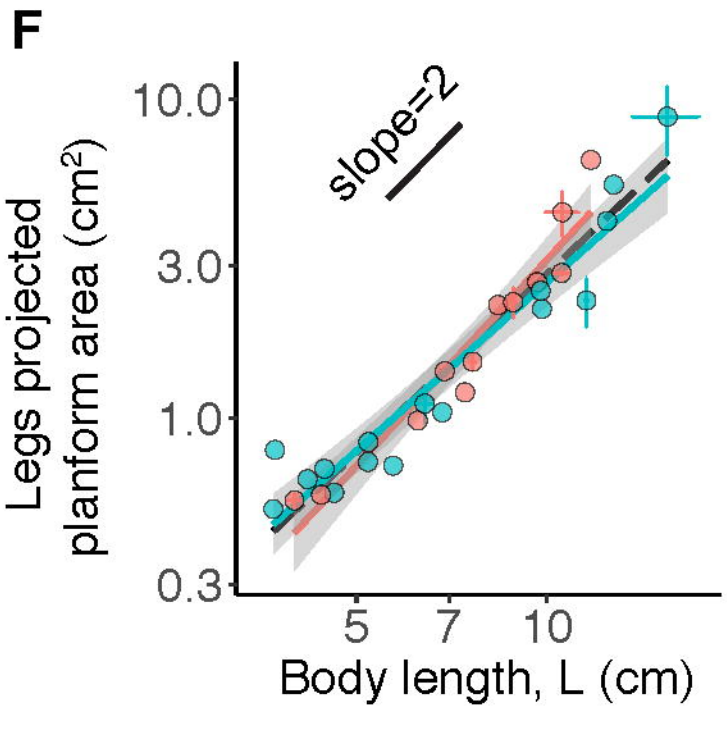

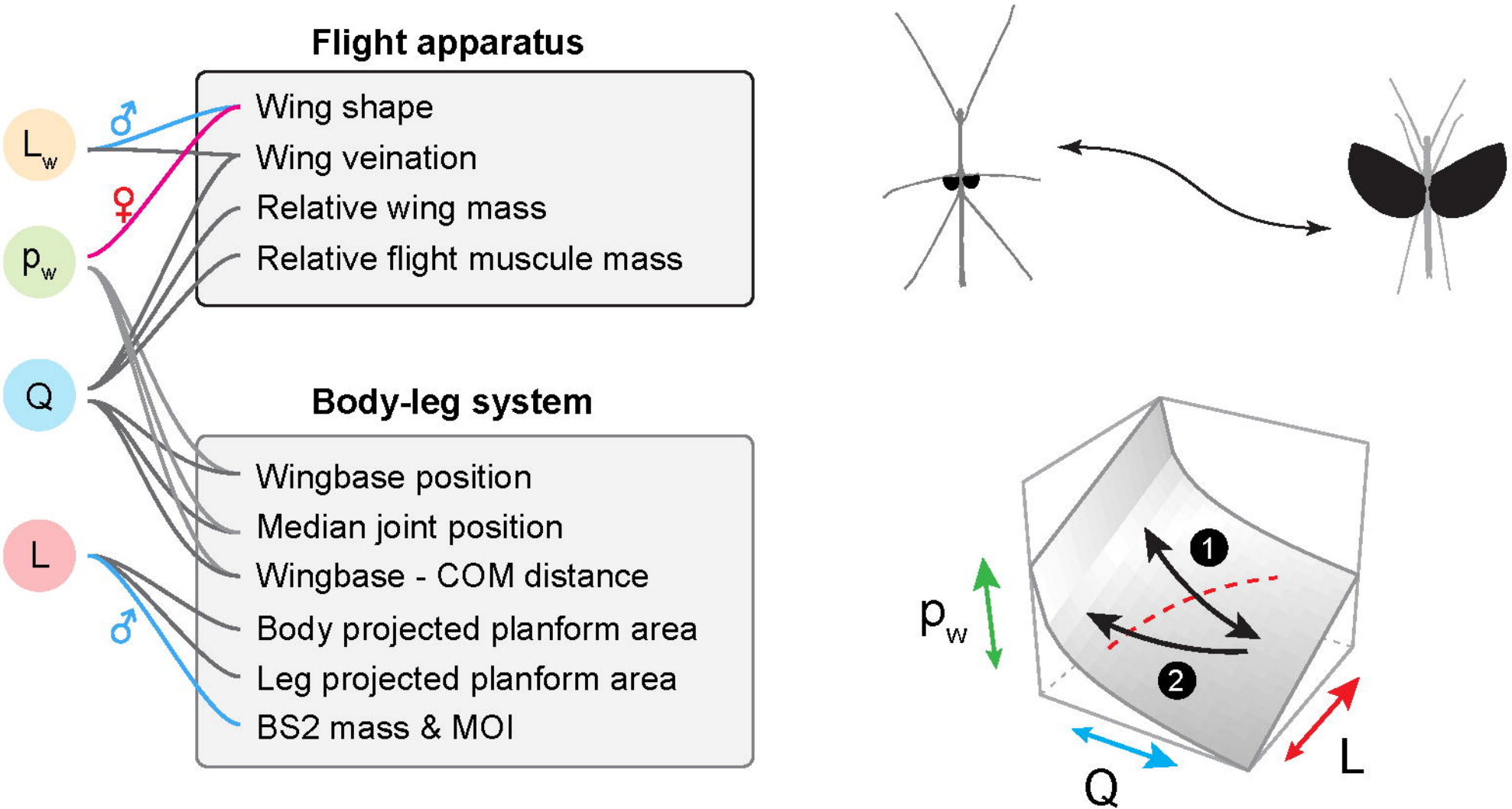
Flight apparatus
Wing shape
Wing veination
Relative wing mass
Relative flight muscule mass
L_w
p_w
Q
L
♂
♀
Body-leg system
Wingbase position
Median joint position
Wingbase - COM distance
Body projected planform area
Leg projected planform area
BS2 mass & MOI
1
2
p_w
Q
L